Therapeutically advantageous secondary targets of abemaciclib identified by multi-omics profiling of CDK4/6 inhibitors

Marc Hafner*,[1], Caitlin E. Mills*,[1], Kartik Subramanian[1], Chen Chen[1], Mirra Chung[1], Sarah A. Boswell[1], Robert A. Everley[1], Charlotte S. Walmsley[2], Dejan Juric[1,2,ϕ], and Peter K. Sorger[1,†,ϕ]

* These authors contributed equally to this work.
ϕ These authors contributed equally to this work.

† Pre-publication correspondence should be addressed to Peter Sorger (peter_sorger@hms.harvard.edu); copying Marc Hafner (marchafner.hms@gmail.com).

[1]Laboratory of Systems Pharmacology
Department of Systems Biology
Harvard Medical School
Boston, MA 02115

[2]Termeer Center for Targeted Therapies
Massachusetts General Hospital Cancer Center
Boston, MA 02114

The authors declare no potential conflicts of interest.

Abstract

Three inhibitors of the cyclin-dependent kinases CDK4/6, palbociclib, ribociclib, and abemaciclib, have emerged as highly promising therapies for the treatment of breast cancer and other solid tumors. These drugs are reported to have similar mechanisms of action although recent data suggest that abemaciclib exhibits distinct single-agent activity and toxicity. We compare their mechanisms of action using biochemical assays, mRNA profiling, mass spectrometry-based phospho-proteomics, and GR-based dose-response assays. We find that abemaciclib has activities not shared by palbociclib or ribociclib including: induction of cell death (even in pRb-deficient cells), arrest in the G2 phase of the cell cycle, and reduced drug adaptation. These activities appear to arise from inhibition of CDKs other than CDK4/6 including CDK2/Cyclin A/E and CDK1/Cyclin B. We propose that inhibition of these kinases by abemaciclib overcomes known mechanisms of resistance to CDK4/6 inhibition and may be therapeutically advantageous for patients whose tumors progress on palbociclib or ribociclib.

Introduction

Progression through the cell cycle is controlled by over a dozen distinct protein complexes involving cyclins and cyclin-dependent kinases (CDKs). Because dysregulation of the cell cycle is a hallmark of cancer, CDK inhibitors have been under development as therapeutics for many years but it is only recently that CDK4/6 inhibitors have emerged as highly promising drugs, particularly in breast cancer. CDK4 and CDK6 bind cyclin D early in the G1 phase of the cell cycle and phosphorylate the retinoblastoma protein (pRb). pRb is subsequently hyperphosphorylated by CDK2/cyclin E relieving its inhibitory activities against transcription factors of the E2F family which allows for S phase entry. Later in the cell cycle, CDK2/cyclin A and CDK1 in complex with either cyclin A or B promote entry and progression through G2 and mitosis. Multiple genetic changes in cancer cells disrupt critical steps in cell cycle regulation: amplification of CDK4, CDK6, cyclin D, or cyclin E are common in solid tumors including breast cancer[1,2]. Deficiency in pRb function, which causes unregulated S phase entry and deletion of CDKN2A, which encodes the CDK4/6 inhibitor p16, are observed across all cancers[2,3].

First generation pan-CDK inhibitors are active against cell cycle regulators such as CDK1/2/4/6 and transcriptional regulators such as CDK7/9. These inhibitors arrest cells in both G1 and G2 and are broadly cytotoxic[2]. Clinical development of CDK inhibitors has been challenging largely because of poor therapeutic windows[2] and lack of selectivity. Subsequent generations of CDK inhibitors are designed to inhibit specific subsets of CDK proteins. In February 2015, the CDK4/6 inhibitor, palbociclib (PD0332991; Ibrance)[4], received FDA approval for the management of hormone receptor-positive (HR^+) metastatic breast cancer[5,6] (MBC). Approval was granted based on results of the PALOMA-1 trial, which demonstrated a significant improvement in progression-free survival of patients who received palbociclib with letrozole, as compared to letrozole alone; and palbociclib has subsequently exhibited activity in other malignancies[7–10]. Subsequent to approval of palbociclib large clinical trials of two other CDK4/6 inhibitors, ribociclib (LEE011; Kisqali)[11] and abemaciclib (LY2835219; Verzenio)[12,13], have reported similar improvements in progression-free survival[4,14] in HR+

MBC, leading to their FDA approval and making CDK4/6 inhibitors some of the most promising new drugs for the treatment of breast cancer.

As observed with many other targeted therapies, however, acquired resistance to CDK4/6 inhibitors develops over time and nearly all initially responsive patients ultimately show disease progression[15]. The emergence of tumors resistant to CDK4/6 inhibitors is associated with multiple genomic alterations including loss of pRb function, amplification of CDK6, and of cyclin E, which promotes CDK2-dependent phosphorylation of pRb, thereby bypassing the requirement for CDK4/6 activity[2,16]. At the single-cell level, high expression of cyclin E has been associated with high CDK2 activity post-mitosis, which appears to bypass a requirement for CDK4/6 for cell cycle reentry[17].

Despite having the same nominal target and similar initial clinical indications, emerging evidence suggests that palbociclib, ribociclib, and abemaciclib have differential profiles in the clinic: abemaciclib has single-agent activities and distinct adverse effects[18]. Currently, it is unknown if these drugs are therapeutically interchangeable and whether progression on one CDK4/6 inhibitor can be overcome by switching to a different inhibitor. The three drugs differ in relative activity against CDK4 and CDK6 and differences in target selectivity have been reported based on *in vitro* screening with ribociclib emerging as the most selective inhibitor and abemaciclib the least[19,20]. The activity of abemaciclib against CDK9 has been reported to be inconsequential[21] whereas inhibition of DYRK/HIPK kinases has been reported to be a possible cause of cytotoxicity[22]. The importance of kinase selectivity in influencing anti-proliferative activity has not been established. All three agents are presented by their manufacturers as being similar in antitumor activity but with some differences in pharmacokinetics and toxicities: abemaciclib is dosed continuously whereas palbociclib and ribociclib are dosed intermittently to ameliorate hematologic toxicity[15].

In this study, we directly compare the targets and biological activities of CDK4/6 inhibitors in multiple breast cancer cell lines using a combination of *in vitro* activity assays, mRNA sequencing, protein mass spectrometry and GR-based sensitivity measures[23]. When integrated, these four

experimental approaches provide complementary insight into drug mechanisms of action. We find that palbociclib, ribociclib, and abemaciclib are distinct with respect to their biological activities, target profiles and ability to induce cytostasis and death in breast cancer cells of varying genotypes. Multiple lines of evidence show that the unique biological activities of abemaciclib arise from inhibition of kinases in addition to CDK4/6, notably CDK1/cyclin B and CDK2/cyclin E/A. Inhibition of these kinases is likely to be therapeutically beneficial and may provide rationale for using abemaciclib in patients whose disease progresses on, or does not respond to palbociclib or ribociclib, potentially including those whose cancers manifest loss of pRb function.

Results

Abemaciclib induces molecular signatures distinct from other CDK4/6 inhibitors

To compare mechanisms of action of palbociclib, ribociclib, and abemaciclib we performed transcriptional profiling (mRNA-seq) on a panel of seven breast cancer cell lines following 6 or 24 hours of drug exposure (Fig. 1a and Supplementary Table S1). In all but pRb-deficient BT-549 cells, treatment with any of the three drugs was associated with a cluster (signature 1; Fig. 1a highlighted in red) of 87 significantly down-regulated genes (FDR < 0.2). When this signature was used to query the Broad Connectivity Map (CMAP)[24], inhibitors of MEK (MAP kinase kinase) and palbociclib itself were the strongest hits (ribociclib and abemaciclib are absent from the CMAP dataset; Fig. 1b and Supplementary Table S2). Signature 1 was enriched in genes of the Reactome set "Cell Cycle" ($p=9.0\times10^{-50}$) and inhibition of MEK is anti-mitogenic in breast cancer cells, promoting arrest at the G1/S transition[25,26]. We conclude that signature 1 reflects cell cycle arrest in G1, which is the expected effect of CDK4/6 inhibitors[5]. In all seven cell lines, including pRb-deficient BT-549 cells, treatment with abemaciclib in the low micromolar range induced a second transcriptional signature (signature 2; cyan cluster in Fig. 1a) that was absent from ribociclib-exposed cells and only weakly present in cells exposed to

palbociclib. When the abemaciclib-specific transcript signature was compared to CMAP, the strongest hit was alvocidib (flavopiridol) and other pan-CDK inhibitors (Fig. 1c and Supplementary Table S3).

To better understand the origins of signature 2, we performed phosphoproteome profiling in MCF7 cells using liquid-chromatography mass spectrometry (LC/MS) with isobaric (TMT) tags[27]. We found that abemaciclib inhibited protein phosphorylation at a substantially greater number of phospho-protein sites than did palbociclib (Fig. 1d, Supplementary Table S4). We used enrichment analysis[28] based on known kinase-substrate relationships (see Methods) to infer the activity of kinases whose down-regulation most likely accounted for the observed changes in the phosphoproteome following abemaciclib treatment. We found the inferred activities of CDK4, CDK6, and Aurora A/B kinases (AURKA/B) to be significantly down-regulated in both palbociclib and abemaciclib-treated cells. In addition, our analyses suggested that the activities of CDK1, CDK2, CaM-kinase II subunit alpha (CAMK2A), TTK, and polo-like kinase 1 (PLK1) are uniquely down-regulated by abemaciclib (Fig. 1e, Supplementary Table S5). Thus, abemaciclib has a range of transcriptional and phospho-protein modulatory activities in breast cancer cells that are distinct from those of ribociclib or palbociclib.

Abemaciclib is active against multiple CDK/cyclin complexes

Inference of kinase activity from phosphoproteome data yields both direct and indirect drug targets and we performed *in vitro* assays to distinguish between them. KINOMEscan profiling against a panel of 468 recombinant kinases confirmed that ribociclib is the most selective CDK4/6 inhibitor and abemaciclib the least (Supplementary Fig. S1 and Table S6)[19,20]. SelectScreen kinase activity and binding assays (Thermo Fisher, see Methods) showed that abemaciclib is the most potent inhibitor of CDK4 and CDK6 and that it is also active against multiple kinases that are weakly inhibited, or not inhibited, by palbociclib or ribociclib (Fig. 2a, Supplementary Fig. S2a and Table S7). These kinases include CDK2/cyclin A/E, CDK1/cyclin B, CDK7/cyclin H, CDK9/cyclin K/T1, GSK-3 beta (GSK3B), CAMK2A, and TTK (Supplementary Fig. S2b), targets that were also identified in transcriptional or

phosphoproteomic signatures. In comparison to the first-generation CDK inhibitor alvocidib, abemaciclib is similar in its activity against CDK2/cyclin A/E and about 10-fold less active against CDK1/cyclin B, CDK7/cyclin H, and CDK9/cyclin K/T1 (potentially explaining the improved toxicity profile of abemaciclib relative to pan-CDK inhibitors), whereas ribociclib and palbociclib are orders of magnitude less potent against these kinases. In general, results from KINOMEscan profiling, SelectScreen assays and in-cell profiling were concordant. Two exceptions were observed: CDK1, which is absent from the KINOMEscan panel, and CDK2, which appears to be a false negative finding, perhaps due to a lack of active CDK2/cyclin A and CDK2/cyclin E complexes[29] in the KINOMEscan assay.

When a drug inhibits multiple targets at different concentrations, as does abemaciclib, it is important to determine which targets are relevant at therapeutically achievable doses. We therefore computed the strength of the mRNA differential expression signatures 1 and 2 (which are associated with G1 arrest and pan-CDK inhibition respectively; Fig. 1b-c) across all drugs, doses, and cell lines six hours after drug treatment (Fig. 2b). We found that the score for signature 1 was high under all treated conditions, except in cells deficient in pRb (Fig. 2b, square data points). Treatment with abemaciclib exhibited high scores for signature 2 at doses of 0.3 μM and above in multiple cell lines, whereas treatment with ribociclib resulted in the lowest scores for signature 2, and palbociclib was associated with intermediate values. A significantly higher pan-CDK inhibitor signature score at 0.3 μM abemaciclib ($P = 2.1 \times 10^{-4}$, ranksum test) is consistent with *in vitro* kinase activity and mass spectrometry data for abemaciclib (Fig. 1e). We conclude that abemaciclib induces molecular responses in cells that are not observed with ribociclib or palbociclib at concentrations as low as 0.3 μM, which is comparable to the maximum serum concentration (C_{max}) achieved in patients of 0.5 μM to 1 μM when active metabolites are included[7,30].

Abemaciclib induces a stronger phenotypic response in breast cancer cells

To compare the biological activities of CDK4/6 inhibitors, we acquired dose-response curves in 34 breast cancer cell lines spanning all clinical subtypes using GR metrics (Fig. 3a and Supplementary Table S8) which correct for differences in cell proliferation rates and distinguish between drug-induced cell cycle arrest and cell death[23,31]. Both palbociclib and abemaciclib elicited cytostatic responses with GR_{50} values in the 10-100 nM range (Supplementary Table S9). Potency was highly correlated between the drugs (Spearman's $\rho = 0.91$, $P = 5.7\times10^{-14}$) with abemaciclib on average 5.5-fold (t-test $P = 5.3\times10^{-7}$) more potent in inducing cytostasis; this difference is consistent with a 3-fold difference in IC_{50} values for CDK4/6 inhibition between palbociclib and abemaciclib as measured *in vitro* by SelectScreen assays (Fig. 2a). Efficacy at low doses as measured by GR values at 0.1 μM varied between 0 (complete cytostasis) and 0.67 (weak growth inhibition) depending on the cell line and was similar for palbociclib and abemaciclib, showing that at these concentrations the drugs only fractionally inhibit cell proliferation. The low-dose response was not observed in pRb-deficient cell lines (yellow lines Fig. 3a) and is likely to be the result of CDK4/6 inhibition.

Abemaciclib elicited a second response at doses greater than 0.3 μM; this response was characterized by negative GR values and cell death (see Methods; Fig. 3a); the higher-dose response was not observed in palbociclib-treated cells nor in the eight cell lines in which GR data were collected for ribociclib. As a result, the complete dose-response behavior of abemaciclib was significantly better fitted in most cell lines by the product of two sigmoidal curves (Fig. 3b, Supplementary Fig. S3, and Methods). This behavior is consistent with inhibition of multiple targets with different potencies. The mid-point of these curves was offset to a similar degree as *in vitro* dose-response curves for CDK4/6 vs. CDK1/2 inhibition (Supplementary Table S7). Overall, abemaciclib was substantially more efficacious than palbociclib in inhibiting and killing pRb-proficient cells of all subtypes, having a GR_{max} value on average 0.52 lower (t-test $P = 4.5\times10^{-9}$; Supplementary Table S9). When we searched a set of 30 cell cycle regulators for those whose mRNA expression levels could discriminate between responsiveness to

palbociclib and abemaciclib in pRb-proficient cell lines, we found that a combination of elevated expression of CDKN1A (p21 – an inhibitor of CDK1/2/4/6), CDKL5 (a cyclin-dependent kinase targeted by abemaciclib and other pan-CDK inhibitors based on KINOMEscan data), CCNE1 (cyclin E1, which has been implicated in palbociclib resistance[15]) and reduced expression of CDK9 (another abemaciclib and pan-CDK inhibitor target) comprised a strong preclinical pharmacogenomic predictor across the 26 cell lines tested ($q^2 = 0.85$, $P = 2.9\times10^{-6}$ by leave-one-out cross validation; Fig. 3c). Thus, abemaciclib has biological activities, including induction of cell death, that are not observed with palbociclib and ribociclib at doses that are well within a clinically accessible range based on human pharmacokinetic data. Abemaciclib also induced cell death in pRb-deficient cell lines at concentrations of 1 μM and above, whereas palbociclib was inactive (Fig. 3a; yellow lines).

Abemaciclib blocks cells in the G2 phase of the cell cycle and prevents adaptive response

Consistent with the known biology of CDK4/6 inhibition, abemaciclib, ribociclib, and palbociclib suppressed pRb phosphorylation and elicited G1 cell cycle arrest (Fig. 3d). The differences in potency observed for these drugs matched the differences in IC_{50} values for inhibition of CDK4/6 in biochemical assays (Fig. 2a). A subset of abemaciclib-treated cells was also arrested in G2 at drug concentrations of 0.3 μM and above (Fig. 3d, Supplementary Fig. S4a), likely due to inhibition of CDK1 and CDK2 whose activities are required for mitotic progression. Unusually, some abemaciclib-treated G2-arrested cells were phospho-pRb positive (p-pRb$^+$). This likely occurred because the cells were blocked prior to entering mitosis and passing through to G1 at which time pRb would normally be dephosphorylated. Treating pRb-deficient cells with ribociclib or palbociclib had no effect on cell cycle distribution whereas treatment with abemaciclib resulted in G2 arrest, again suggesting abemaciclib-induced inhibition of CDK1/2 (Fig. 3e, Supplementary Fig. S4a,b).

Within 48 hours of continuous exposure to palbociclib or ribociclib, pRb-proficient cells re-acquired a p-pRb$^+$ state even at a high drug concentration (3.16 μM), consistent with previous data

showing that cells can escape from cytostasis induced by CDK4/6 inhibition (Fig. 3d)[17,32]. In contrast, pRb phosphorylation remained low in cells exposed to 1 μM abemaciclib (Fig. 3d) with ongoing cell death and no evidence of adaptation with up to five days of continuous exposure (Fig. 4a, Supplementary Fig. S5 and Table S10). In studies designed to assess long-term adaptation to drug, we observed that breast cancer cells grown for several months in the presence of 1 μM palbociclib had lower pRb and higher cyclin E levels than parental cells; these changes are expected to make cells relatively resistant to CDK4/6 inhibition (Fig. 4b). Palbociclib-adapted cells were cross-resistant to ribociclib (Fig. 4c, Supplementary Fig. S6 and Table S11). In contrast, palbociclib-adapted cells were sensitive to abemaciclib at doses of 1 μM and above, consistent with the ability of abemaciclib to target multiple kinases not inhibited by palbociclib.

Are mechanisms of action of abemaciclib other than CDK4/6 inhibition of therapeutic significance? To begin to address this question, we established a cell line from a patient with advanced/metastatic HR^+/Her2- breast cancer whose disease had progressed following eight months on ribociclib/letrozole. The tumor lacked pRb by immunohistochemistry (Supplementary Fig. S7a) as did the derived cell line (MGH312; Supplementary Fig. S7b). These tumor cells were responsive to abemaciclib as judged by inhibition of cell proliferation and induction of cell death but were completely resistant to palbociclib or ribociclib even at high doses (Fig. 4f and Supplementary Table S12). While we cannot prove that this patient would have benefited from treatment with abemaciclib, the data suggest that abemaciclib may be active on tumors that have become resistant to other CDK4/6 inhibitors, providing rationale for trials of abemaciclib in post-palbociclib or -ribociclib HR+ settings including in patients with RB1-mutated tumors.

Discussion

The demonstration that CDK4/6 inhibitors are effective for the treatment for HR+ metastatic breast cancer has resulted in over 100 clinical trials of palbociclib, ribociclib and abemaciclib in multiple

malignancies. It has been assumed that the mechanisms of action of the three drugs are the same and that any discrepancies in efficacy and toxicity are due to differences in dosing schedules and relative potencies against CDK4 vs. CDK6. However, four lines of evidence in our work demonstrate that abemaciclib has activities not manifest by ribociclib and only weakly by palbociclib. First, treatment of breast cancer cells of different genotypes with abemaciclib induces not only transcriptional changes associated with G1 arrest, a property shared by palbociclib and ribociclib, but also induces changes in transcription that closely resemble the CMAP signatures for pan-CDK inhibitors such as alvocidib. Second, exposing cells to abemaciclib results in more extensive changes in the phosphoproteome than exposure to palbociclib; kinase inference suggests that this is due in part to inhibition of CDK1 and CDK2 activity by abemaciclib. *In vitro* kinase assays confirm that CDK1/2 are direct targets of abemaciclib, placing abemaciclib, in regards to target selectivity, between the highly selective CDK4/6 inhibitors such as ribociclib and the first generation CDK inhibitors. Third, abemaciclib causes arrest of cells in both the G1 and G2 phases of the cell cycle and the drug is cytotoxic even in the absence of pRb; in contrast, cells exposed to palbociclib and ribociclib arrest only in G1 and cause little or no cell death. Fourth, whereas abemaciclib durably inhibits cell proliferation, cultured cells adapt within 2-3 days of continuous exposure to palbociclib or ribociclib and resume proliferation.

Our results argue for a multi-faceted approach to the identification of kinase inhibitor targets. Proteomic, transcriptional, biochemical, and phenotypic assays measure different aspects of cancer cell physiology and their use in combination was necessary in the current example for a complete picture of drug mechanisms of action. Proteomic and mRNA profiling showed that exposure of breast cancer cells to abemaciclib results in inhibition of CDK9, Aurora A/B kinases (AURKA/B), CaM-kinase II subunit alpha (CAMK2A), TTK, and polo-like kinase 1 (PLK1). Biochemical experiments showed that AURKA/B and PLK1 are most likely indirect targets of abemaciclib down-regulated as a consequence of G2 cell cycle arrest, whereas CAMK2A and TTK are direct targets of abemaciclib. Inhibition of GSK3B was observed in biochemical assays but was borderline significant by phosphoproteomic

analysis, perhaps reflecting the challenges of inferring changes in kinase activity from data that are inherently under-sampled[33]. The false negative finding in the widely used KINOMEscan data that abemaciclib does not interact with CDK2, may explain why biologic differences among CDK4/6 inhibitors are not widely appreciated.

In the case of a poly-selective drug such as abemaciclib it is important to determine the dose range at which inhibition of different targets is clinically relevant. There is no question that abemaciclib is the most potent of the three drugs against CDK4 and CDK6; biochemical and cell-based data show that abemaciclib inhibits these kinases at a lower concentration than either palbociclib or ribociclib do. Relative to CDK4/6, abemaciclib is 10- to 100-fold less potent against CDK2 and CDK1, but we detect the cellular consequences of CDK1/2 inhibition at a concentration of 0.3 μM, well within its C_{max} range in humans[7,30]. Moreover, cells adapted to grow in the presence of palbociclib in culture, and cells from a patient whose disease progressed on ribociclib/letrozole still respond to abemaciclib. Abemaciclib is active in pRb-deficient cells at concentrations of 1 μM and above, but this activity is not observed with palbociclib or ribociclib. Given the concentrations required, it is not yet clear whether the activity of abemaciclib in pRb-deficient cells will translate into patients; clinical evaluation of RB1-mutant tumors will be required.

The current generation of CDK4/6 inhibitors benefits from a considerable investment in increasing selectivity, mainly as a means of reducing toxicity relative to earlier generation drugs[2,34,35]. The remaining activity of abemaciclib against kinases other than CDK4/6 is likely to be of therapeutic benefit: blocking CDK2/cyclin E should mitigate resistance resulting from amplification of cyclin E[32,36] and achieve a more complete response by targeting cells exiting mitosis with high CDK2 activity[17]; inhibition of CDK1/7/9 may also contribute to cell killing[37,38]; inhibition of mitotic kinases such as TTK may enhance tumor immunogenicity, a key contributor to drug response[39]; and pRb-independent anti-proliferative effects may reduce resistance stemming from pRb loss of function. These findings imply that it may ultimately be useful to select patients for abemaciclib treatment based on enhanced activity

of CDK1/2[17] and/or loss of pRb. Abemaciclib may also be valuable in a post-palbociclib or post-ribociclib therapeutic setting and in other indications such as triple negative breast cancer.

Methods

Cell culture

Cell lines were purchased from ATCC, and verified by STR profiling[40]. MCF7, and Hs 578T were maintained in Dulbecco's modified Eagle's medium (DMEM), T47D, BT-549, HCC1419 and HCC1806 in Roswell Park Memorial Institute medium (RPMI), and BT-20 in Eagle's minimum essential medium (EMEM) supplemented in each case with 10% heat-inactivated fetal bovine serum (FBS) and 1% penicillin-streptomycin (P/S). Cells were tested routinely for mycoplasma. The PDX12-58 and HCI002 cultures were kindly provided by D. Stover and J. Brugge, and maintained in F-media containing ROCK inhibitor as described[41] with 1% P/S instead of gentamycin and fungizone. The MGH312 cell line was established as described[42] by direct culture of patient biopsy material, and initially plated in ACL4 with 5% FBS and 1% Antibiotic-Antimycotic. Once 100% tumor cellularity was achieved, the cells were transitioned to and maintained in RPMI with 10% FBS and 1% P/S. All cells were grown at 37°C, and 5% CO_2.

Dose response measurements

Cells were plated at densities ranging from 500 to 2000 cells per well in 384-well Cell Carrier plates (Perkin Elmer, Waltham, MA) using a Multidrop Combi Reagent Dispenser (Thermo Fisher Scientific, Waltham, MA) and grown for 36 hours. Cells were treated with a dilution series of the indicated drugs by pin transfer or using a D300 Digital Dispenser (Hewlett-Packard, Palo Alto, CA). Drugs were obtained from commercial vendors and tested for purity in-house as described in detail in the HMS LINCS drug collection database (http://lincs.hms.harvard.edu/db/sm/). Cells were stained and fixed for analysis at the time of drug delivery and after 24 to 144 hours of incubation depending on the experiment. Cells were stained at the indicated time points with 2 µg/ml Hoechst 33342 (Sigma Aldrich, St. Louis, MO) and 1:1000 LIVE/DEAD Far Red Dead Cell Stain (Thermo Fisher Scientific, Waltham, MA) for 30 minutes and fixed with 3.7% formaldehyde (Sigma Aldrich, St. Louis, MO) for 30 minutes. Fixed cells were imaged with a 10x objective using an Operetta microscope and analyzed using the Columbus image data storage and analysis system (Perkin Elmer, Waltham, MA). For most

experiments, each condition was tested across three replicate plates and at least four wells per cell line per plate were untreated.

Nuclei counts were normalized to DMSO-treated controls on the same plate to yield relative cell count and normalized growth rate inhibition (GR) values for each technical replicate for each condition as described previously[23]. Technical replicates were averaged to yield mean relative cell counts and the mean GR value for each condition within each biological replicate. Within each biological replicate, mean GR values for a given cell line / small molecule combination across all tested concentrations were fitted to a biphasic sigmoidal curve with the equation:

$$GR(c) = 2^{\log_2\left(GR_{max}^{1st}+\frac{1-GR_{max}^{1st}}{1+\left(c/GEC_{50}^{1st}\right)^{h^{1st}}}+1\right)\cdot\log_2\left(GR_{max}^{2nd}+\frac{1-GR_{max}^{2nd}}{1+\left(c/GEC_{50}^{2nd}\right)^{h^{2nd}}}+1\right)} - 1,$$

or with a single sigmoidal curve with the equation:

$$GR(c) = GR_{max} + \frac{1 - GR_{max}}{1 + \left(c/GEC_{50}\right)^{h}} + 1,$$

or with a flat line with the equation $GR(c) \equiv GR_{max}$. The significance of each curve was assessed using an F-test and the most complex model with $P < 0.05$ was considered to best fit the data. The parameters of the sigmoidal curve and the first phase of the biphasic curve are constrained as described in Hafner *et al.*[43]. In the biphasic curve, the parameter GEC_{50}^{2nd} is constrained to be above 0.3 µM. The time-dependent GR values for Fig. 4a were evaluated over a 48-hour interval using the formula described previously[23].

Phospho-pRb immunofluorescence and cell cycle analysis

Cells were seeded in 384-well plates, allowed to adhere for 24-36 hours, treated with CDK4/6 inhibitors, incubated for the desired amount of time then fixed in 4% formaldehyde, permeabilized with 0.5% Triton X-100 in PBS, and blocked with Odyssey blocking buffer (LI-COR, Lincoln, NE). Cells were labeled overnight at 4°C with a 1:800 dilution of anti-phospho-pRb Alexa-555 (Ser807/811) (Cell Signaling Technologies, Danvers, MA) and 2 µg/ml Hoechst 33342 (Sigma Aldrich, St. Louis, MO) prepared in Odyssey blocking buffer. Images were acquired with a Perkin Elmer Operetta microscope as described for the dose response measurements. Nuclei were segmented using Columbus software (Perkin Elmer, Waltham, MA) based on their Hoechst signal. DNA content was defined by the total Hoechst intensity within the nuclear mask. The average phospho-pRb intensity within the nuclear mask was determined, and a threshold for positivity was set by visually inspecting images of several control and treated wells per cell line.

mRNA-seq

Cells were seeded in 12-well plates, and allowed to adhere for 24 hours at which time CDK4/6 inhibitors were added. Cells were lysed in the plates after 6 or 24 hours, and RNA was extracted using Applied Biosystems MagMax 96 total RNA isolation kit (Thermo Fisher Scientific, Waltham, MA) with DNAse digestion according to the manufacturer's protocol. RNA was checked for quantity with a NanoDrop (Thermo Fisher Scientific, Waltham, MA) and for quality using an Agilent Bioanalzyer instrument (with RIN value > 9.0). Libraries were prepared using a TruSeq Stranded mRNA sample preparation kit (Illumina, San Diego, CA) from 500 ng of purified total RNA according to the manufacturer's protocol in a reduced reaction volume. The finished cDNA libraries were assessed for quality using a Bioanalyzer and quantified with a Quant-iT dsDNA Assay kit (Thermo Fisher Scientific, Waltham, MA). The uniquely indexed libraries were multiplexed based on this quantitation and the pooled sample was quantified by qPCR using the Kapa Biosystems (Wilmington, MA) library quantification kit by the Molecular Biology Core Genomics Facility at the Dana-Farber Cancer Institute and sequenced on a single Illumina NextSeq500 run with single-end 75bp reads.

Reads were processed to counts through bcbio-Nextgen toolkit (https://github.com/chapmanb/bcbio-nextgen) 1.0.3a as follow: (1) Reads were trimmed and clipped for quality control in cutadapt v1.12; (2) Read quality was checked for each sample using FastQC 0.11.5; (3) High-quality reads were then align into BAM files through STAR 2.5.3a using the human assembly GRCh37; (4) BAM files were imported into DEXSeq-COUNT 1.14.2 and raw counts TPM and RPKM were calculated. R package edgeR[44] 3.18.1 (R version 3.2.1) was used for differential analysis and generate log fold change, *P*-value and FDR.

Clustering analysis of the mRNA-seq data and L1000 signatures

Differential gene expression signatures were clustered along samples and genes based on the cosine distance for the log2(fold-change) using MATLAB default functions. log2(fold-change) values for genes with FDR values above 0.2 were set to zero. In figure 1a, the down-regulated gene clusters were defined manually based on the dendrogram of the genes. Each set of genes was used to query the set 'LINCS_L1000_Chem_Pert_down' in Enrichr[45] (see Supplementary Table 2 and 3). Enrichment analysis was performed using the GSEA algorithm (gsea2-2.2.3.jar from Broad Institute[46]) on the results used sets based on the name of 31 well-annotated drugs with $-\log_{10}$(*P*-value) as weight and the results was plotted in Fig. 1b,c.

Phosphoproteomics mass spectrometry

MCF7 cells were treated with 0.3 μM and 3 μM of palbociclib or abemacicblib or DMSO control for 1 hour in duplicate. For each sample, 4.5 mg of protein was utilized to perform serine and threonine phosphoproteome analysis. The samples were digested using Trypsin (Promega, Madison, WI), acidified and desalted using C18 Sep-Pak (Waters, Milford, MA). Phosphopeptides were enriched using the Thermo Scientific High-Select Fe-NTA Phosphopeptide Enrichment Kit. TMT was added as previously described[47,48]. The sample was then enriched for phosphotyrosine-containing peptides using the pY-1000 antibody (Cell Signaling Technologies, Danvers, MA) coupled to Pierce Protein A Agarose beads (Thermo Fisher Scientific, Waltham, MA). The flow-through from the pY sample was kept and desalted for pS and pT analysis. 24 fractions (phosphoproteomics) were then desalted using the C18 StageTip procedure[49]. All MS analyses were performed on an Orbitrap Fusion Lumos mass spectrometer (Thermo Fisher Scientific, Waltham, MA) using a multi-notch MS3 method[50,51]. Raw data were converted to mzXML and searched via Sequest[52] version 28 against a concatenated Uniprot database (downloaded 02/04/2014). Linear discriminate analysis was used to distinguish forward and reverse hits and reverse hits were filtered to an FDR of 1% at the protein level. Site localization confidence was assessed using the A-score method[53]. Reporter ion intensities were quantified and normalized as described earlier[48].

Annotation of phosphopeptides with upstream kinases

16,300 phosphopeptides were detected across all conditions in MCF7 cells. The PhosphoSitePlus (PSP) database[54], which contains curated annotations of upstream kinases, was queried using phosphopeptide sequence motifs and UniProt IDs as identifiers. Only ~6.3% of the phosphopeptides detected by phosphoproteomics had experimentally verifiable kinase annotations on PSP. The NetworKIN algorithm[55] that predicts upstream kinases, based on phosphopeptide sequences and STRING evidence, was used to identify kinases for the remaining phosphosites. A further 14% of phosphosites were annotated with predicted kinases (NetworKIN Score > 4). In total, 3145 phosphopeptides from 1242 proteins were annotated as being phosphorylated by 365 kinases (8297 kinase-peptide interaction pairs).

Differential kinase activity score using GSEA

Based on the method described previously[28], a kinase set library was assembled using the identified kinase-substrate relationships. The kinase set library is composed of kinases and their

corresponding sets of phosphopeptide substrates. Only kinase sets that had more than 25 downstream phosphosites were used. The final kinase set library was composed of 60 kinases that phosphorylate 2597 peptides. For each phosphopeptide, the mean difference between the replicates and the maximum difference across conditions were computed. If the delta between the two scores was less than 1, then the phosphopeptide measurement was considered noisy and discarded, resulting in a final list of 9958 phosphopeptides (Supplementary Table 4). For each of the four treatment conditions, the average log2 (fold-change) was computed relative to the untreated control. Using the phosphopeptide log2(fold-change) values as input and the final kinase set library, GSEA algorithm (gsea2-2.2.3.jar from Broad Institute[46]) was used to infer the enrichment score ($P < 0.05$ and FDR < 0.2). The enrichment score is a proxy metric for the differential activity of the kinases.

In vitro measurement of kinase inhibitory activity.

Ribociclib, palbociclib, and abemaciclib were assayed using the KINOMEscan® assay platform (DiscoverX, Fremont, CA). Data are reported as percent of remaining activity at either 0.1 or 1.0 μM drug concentration.

The activity of ribociclib, palbociclib, abemaciclib, and alvocidib on multiple CDK-cyclin complexes and other kinases were assayed using Thermo Fisher Scientific SelectScreen Kinase Profiling service. The 'Adapta™' assay was used for CDK4/cyclin D1, CDK4/cyclin D3, CDK6/cyclin D1, CDK7/cyclin H/MNAT1, and CDK9/cyclin T1. The 'LanthaScreen™' Kinase Binding assay was used for CDK2/cyclin A1, CDK2/cyclin E1, CDK9/cyclin K, and TTK. The 'Z′-LYTE™' assay was used for CDK1/cyclin B, AURKA, AURKB, CAMK2A, GSK3B, and PLK1. The ATP concentration was Km[app] when available or 10μM otherwise.

Western blots

20 μg of whole cell lysate (Fig. 4) or 12 μg of whole cell lysate (Supplementary Fig. S7), prepared in M-PER lysis buffer (Thermo Fisher Scientific, Waltham, MA) with complete protease inhibitor cocktail (Sigma Aldrich, St. Louis, MO), was added per well in Mini-PROTEAN TGX precast gels (Bio-Rad, Hercules, CA). Primary mouse monoclonal pRb, cyclin E, and β-actin antibodies were used at 1:1000 dilutions. Secondary anti-mouse IgG, HRP-linked was used 1:2000. All antibodies were from Cell Signaling Technologies (Danvers, MA).

Immunohistochemistry

A 4 μm slice of a formalin-fixed, paraffin-embedded, biopsy of the liver lesion from which the MGH312 cell line was derived was mounted on a standard glass slide and stained for RB expression using a Leica Bond autostainer. The primary Rb antibody (clone 1F8; Bio SB, Santa Barbara, CA) was diluted 1:500 in Leica Bond Diluent and incubated for 15 min. The slide was counterstained with hematoxylin.

Identifying genes associated with differential efficacy of abemaciclib and palbociclib

Using the baseline mRNA expression of 30 genes linked to the cell cycle (cyclins, CDKs, CDKLs, and CDKNs), we built a multilinear model (MATLAB function 'fitglm') to predict the difference in GR values at 3.2 μM between palbociclib and abemaciclib for the pRb-proficient cell lines profiled in Fig. 3a. Predictors with non-significant coefficients ($P > 0.05$) were iteratively removed until only significant coefficients remained. A leave-one-out cross validation was performed with the remaining predictors to yield the results in Fig. 3c. Note that results were qualitatively similar if the pRb-deficient cell lines were included.

Acknowledgements. This work was funded by P50GM107618 and U54HL127365 to PKS and DJ. We thank LSP member M. Berberich for skilled assistance, the ICCB for help with automation, S. Gygi for use of software and computing facilities for proteomics, and A. Bardia for comments.

Author contributions. MH, CEM, and DJ conceived the study; MH, CEM, DJ, and PKS designed the experiments and CEM, MC, SAB, and RAE performed them. MH, KS, and CC performed the computational analyses. CSW and DJ obtained the patient-derived line and provided related data. PKS oversaw the experimental and computational research; MH, CEM, KS, DJ, and PKS wrote the manuscript.

References

1. Balko, J. M. *et al.* Molecular profiling of the residual disease of triple-negative breast cancers after neoadjuvant chemotherapy identifies actionable therapeutic targets. *Cancer Discov.* **4,** 232–45 (2014).

2. Asghar, U., Witkiewicz, A. K., Turner, N. C. & Knudsen, E. S. The history and future of targeting cyclin-dependent kinases in cancer therapy. *Nat. Rev. Drug Discov.* **14,** 130–146 (2015).

3. Franco, J., Witkiewicz, A. K. & Knudsen, E. S. CDK4/6 inhibitors have potent activity in combination with pathway selective therapeutic agents in models of pancreatic cancer. *Oncotarget* **5,** 6512–6525 (2014).

4. Cristofanilli, M. *et al.* Fulvestrant plus palbociclib versus fulvestrant plus placebo for treatment of hormone-receptor-positive, HER2-negative metastatic breast cancer that progressed on previous endocrine therapy (PALOMA-3): final analysis of the multicentre, double-blind, phas. *Lancet. Oncol.* **17,** 425–39 (2016).

5. O'Leary, B., Finn, R. S. & Turner, N. C. Treating cancer with selective CDK4/6 inhibitors. *Nat. Rev. Clin. Oncol.* **13,** 417–430 (2016).

6. Finn, R. S. *et al.* PD 0332991, a selective cyclin D kinase 4/6 inhibitor, preferentially inhibits proliferation of luminal estrogen receptor-positive human breast cancer cell lines in vitro. *Breast Cancer Res.* **11,** R77 (2009).

7. Patnaik, A. *et al.* Efficacy and Safety of Abemaciclib, an Inhibitor of CDK4 and CDK6, for Patients with Breast Cancer, Non–Small Cell Lung Cancer, and Other Solid Tumors. *Cancer Discov.* **6,** (2016).

8. Lim, J. S. J., Turner, N. C. & Yap, T. A. CDK4/6 Inhibitors: Promising Opportunities beyond Breast Cancer. *Cancer Discov.* **6,** 697–9 (2016).

9. Goel, S. *et al.* Overcoming Therapeutic Resistance in HER2-Positive Breast Cancers with CDK4/6 Inhibitors. *Cancer Cell* **29,** 255–69 (2016).

10. McCain, J. First-in-Class CDK4/6 Inhibitor Palbociclib Could Usher in a New Wave of Combination Therapies for HR+, HER2- Breast Cancer. *P T* **40,** 511–20 (2015).

11. Hortobagyi, G. N. *et al.* Ribociclib as First-Line Therapy for HR-Positive, Advanced Breast Cancer. *N. Engl. J. Med.* **375,** 1738–1748 (2016).

12. Dickler, M. N., Tolaney, S. M., Rugo, H. S. & Cortes, J. MONARCH1: Results from a phase II study of abemaciclib, a CDK4 and CDK6 inhibitor, as monotherapy, in patients with HR+/HER2- breast cancer, after chemotherapy for advanced disease. *J Clin Oncol 34* **34,** (2016).

13. Sledge, G. W. *et al.* MONARCH 2: Abemaciclib in Combination With Fulvestrant in Women With HR+/HER2- Advanced Breast Cancer Who Had Progressed While Receiving Endocrine Therapy. *J. Clin. Oncol.* JCO2017737585 (2017). doi:10.1200/JCO.2017.73.7585

14. Griggs, J. J. & Wolff, A. C. Cyclin-Dependent Kinase 4/6 Inhibitors in the Treatment of Breast Cancer: More Breakthroughs and an Embarrassment of Riches. *J. Clin. Oncol.* JCO2017739375 (2017). doi:10.1200/JCO.2017.73.9375

15. Sherr, C. J., Beach, D. & Shapiro, G. I. Targeting CDK4 and CDK6: From Discovery to Therapy. *Cancer Discov.* **6,** 353–67 (2016).

16. Yang, C. *et al.* Acquired CDK6 amplification promotes breast cancer resistance to CDK4/6 inhibitors and loss of ER signaling and dependence. *Oncogene* **36,** 2255–2264 (2017).

17. Asghar, U. S. *et al.* Single-Cell Dynamics Determines Response to CDK4/6 Inhibition in Triple-Negative Breast Cancer. *Clin. Cancer Res.* **23,** 5561–5572 (2017).

18. Patnaik, A., Rosen, L. S., Tolaney, S. M., Tolcher, A. W. & Goldman, J. W. Single-Agent Abemaciclib Active in Breast Cancer. *Cancer Discov.* **6,** 809–10 (2016).

19. Chen, P. *et al.* Spectrum and Degree of CDK Drug Interactions Predicts Clinical Performance. 1–11 (2016). doi:10.1158/1535-7163.MCT-16-0300

20. Gelbert, L. M. *et al.* Preclinical characterization of the CDK4/6 inhibitor LY2835219: in-vivo cell cycle-dependent/independent anti-tumor activities alone/in combination with gemcitabine. *Invest.*

New Drugs **32,** 825–37 (2014).

21. Torres-guzmán, R. *et al.* Preclinical characterization of abemaciclib in hormone receptor positive breast cancer. (2017).

22. Knudsen, E. S. *et al.* Biological specificity of CDK4/6 inhibitors: dose response relationship, *in vivo* signaling, and composite response signature. *Oncotarget* **8,** 43678–43691 (2017).

23. Hafner, M., Niepel, M., Chung, M. & Sorger, P. K. Growth rate inhibition metrics correct for confounders in measuring sensitivity to cancer drugs. *Nat. Methods* **13,** 521–527 (2016).

24. Lamb, J. *et al.* The Connectivity Map: using gene-expression signatures to connect small molecules, genes, and disease. *Science* **313,** 1929–35 (2006).

25. Meloche, S. & Pouysségur, J. The ERK1/2 mitogen-activated protein kinase pathway as a master regulator of the G1- to S-phase transition. *Oncogene* **26,** 3227–3239 (2007).

26. Caunt, C. J., Sale, M. J., Smith, P. D. & Cook, S. J. MEK1 and MEK2 inhibitors and cancer therapy: the long and winding road. *Nat. Rev. Cancer* **15,** 577–92 (2015).

27. McAlister, G. C. *et al.* Increasing the multiplexing capacity of TMTs using reporter ion isotopologues with isobaric masses. *Anal. Chem.* **84,** 7469–78 (2012).

28. Drake, J. M. *et al.* Oncogene-specific activation of tyrosine kinase networks during prostate cancer progression. *Proc. Natl. Acad. Sci.* (2012). doi:10.1073/pnas.1120985109

29. Echalier, A., Hole, A. J., Lolli, G., Endicott, J. A. & Noble, M. E. M. An inhibitor's-eye view of the atp-binding site of CDKs in different regulatory states. *ACS Chem. Biol.* **9,** 1251–1256 (2014).

30. Burke, T. *et al.* Abstract 2830: The major human metabolites of abemaciclib are inhibitors of CDK4 and CDK6. *Cancer Res.* **76,** 2830–2830 (2016).

31. Hafner, M., Niepel, M. & Sorger, P. K. Alternative drug sensitivity metrics improve preclinical cancer pharmacogenomics. *Nat. Biotechnol.* **35,** 500–502 (2017).

32. Herrera-Abreu, M. T. *et al.* Early Adaptation and Acquired Resistance to CDK4/6 Inhibition in Estrogen Receptor–Positive Breast Cancer. *Cancer Res.* **76,** 2301–2313 (2016).

33. Riley, N. M. & Coon, J. J. Phosphoproteomics in the Age of Rapid and Deep Proteome Profiling. *Anal. Chem.* **88,** 74–94 (2016).

34. Toogood, P. L. *et al.* Discovery of a potent and selective inhibitor of cyclin-dependent kinase 4/6. *J. Med. Chem.* **48,** 2388–2406 (2005).

35. Peplow, M. Astex shapes CDK4/6 inhibitor for approval. *Nat. Biotechnol.* **35,** 395–396 (2017).

36. Dean, J. L., Thangavel, C., McClendon, A. K., Reed, C. A. & Knudsen, E. S. Therapeutic CDK4/6 inhibition in breast cancer: key mechanisms of response and failure. *Oncogene* **29,** 4018–32 (2010).

37. Kitada, S., Zapata, J. M., Andreeff, M. & Reed, J. C. Protein kinase inhibitors flavopiridol and 7-hydroxy-staurosporine down-regulate antiapoptosis proteins in B-cell chronic lymphocytic leukemia. *Blood* **96,** 393–397 (2000).

38. Wittmann, S. *et al.* Flavopiridol down-regulates antiapoptotic proteins and sensitizes human breast cancer cells to epothilone B-induced apoptosis. *Cancer Res.* **63,** 93–99 (2003).

39. Luen, S., Virassamy, B., Savas, P., Salgado, R. & Loi, S. The genomic landscape of breast cancer and its interaction with host immunity. *Breast* **29,** 241–250 (2016).

40. Reid, Y., Storts, D., Riss, T. & Minor, L. *Authentication of Human Cell Lines by STR DNA Profiling Analysis*. *Assay Guidance Manual* (2004).

41. Palechor-Ceron, N. *et al.* Radiation Induces Diffusible Feeder Cell Factor(s) That Cooperate with ROCK Inhibitor to Conditionally Reprogram and Immortalize Epithelial Cells. *Am. J. Pathol.* **183,** 1862–1870 (2013).

42. Crystal, A. S. *et al.* Patient-derived models of acquired resistance can identify effective drug combinations for cancer. *Science (80-.).* **346,** 1480 LP-1486 (2014).

43. Hafner, M., Niepel, M., Subramanian, K. & Sorger, P. K. Designing Drug-Response Experiments and Quantifying their Results. *Curr. Protoc. Chem. Biol.* **9,** (2017).

44. Robinson, M. D., McCarthy, D. J. & Smyth, G. K. edgeR: a Bioconductor package for differential

expression analysis of digital gene expression data. *Bioinformatics* **26,** 139–140 (2010).

45. Kuleshov, M. V. *et al.* Enrichr: a comprehensive gene set enrichment analysis web server 2016 update. *Nucleic Acids Res.* **44,** W90–W97 (2016).

46. Subramanian, A. *et al.* Gene set enrichment analysis: A knowledge-based approach for interpreting genome-wide expression profiles. *Proc. Natl. Acad. Sci.* **102,** 15545–15550 (2005).

47. Kettenbach, A. N. & Gerber, S. A. Rapid and Reproducible Single-Stage Phosphopeptide Enrichment of Complex Peptide Mixtures: Application to General and Phosphotyrosine-Specific Phosphoproteomics Experiments. *Anal. Chem.* **83,** 7635–7644 (2011).

48. Paulo, J. A. *et al.* Effects of MEK inhibitors GSK1120212 and PD0325901 in vivo using 10-plex quantitative proteomics and phosphoproteomics. *Proteomics* **15,** 462–73 (2015).

49. Rappsilber, J., Mann, M. & Ishihama, Y. Protocol for micro-purification, enrichment, pre-fractionation and storage of peptides for proteomics using StageTips. *Nat. Protoc.* **2,** 1896–906 (2007).

50. Ting, L., Rad, R., Gygi, S. P. & Haas, W. MS3 eliminates ratio distortion in isobaric multiplexed quantitative proteomics. *Nat. Methods* **8,** 937–40 (2011).

51. McAlister, G. C. *et al.* MultiNotch MS3 enables accurate, sensitive, and multiplexed detection of differential expression across cancer cell line proteomes. *Anal. Chem.* **86,** 7150–8 (2014).

52. Eng, J. K., McCormack, A. L. & Yates, J. R. An approach to correlate tandem mass spectral data of peptides with amino acid sequences in a protein database. *J. Am. Soc. Mass Spectrom.* **5,** 976–89 (1994).

53. Beausoleil, S. A., Villén, J., Gerber, S. A., Rush, J. & Gygi, S. P. A probability-based approach for high-throughput protein phosphorylation analysis and site localization. *Nat. Biotechnol.* **24,** 1285–92 (2006).

54. Hornbeck, P. V. *et al.* PhosphoSitePlus: A comprehensive resource for investigating the structure and function of experimentally determined post-translational modifications in man and mouse.

Nucleic Acids Res. **40,** (2012).

55. Horn, H. *et al.* KinomeXplorer: an integrated platform for kinome biology studies. *Nat. Methods* **11,** 603–4 (2014).

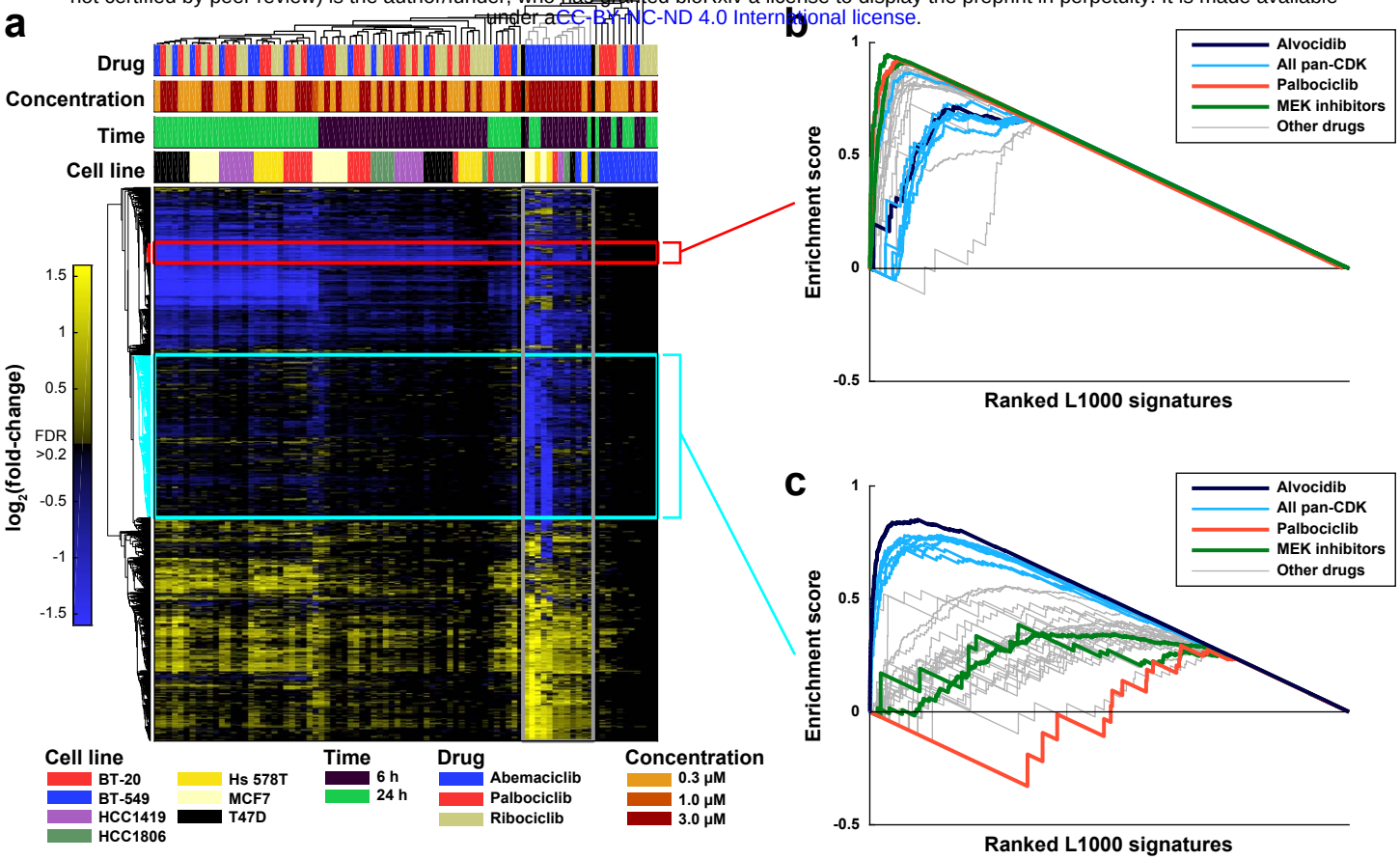

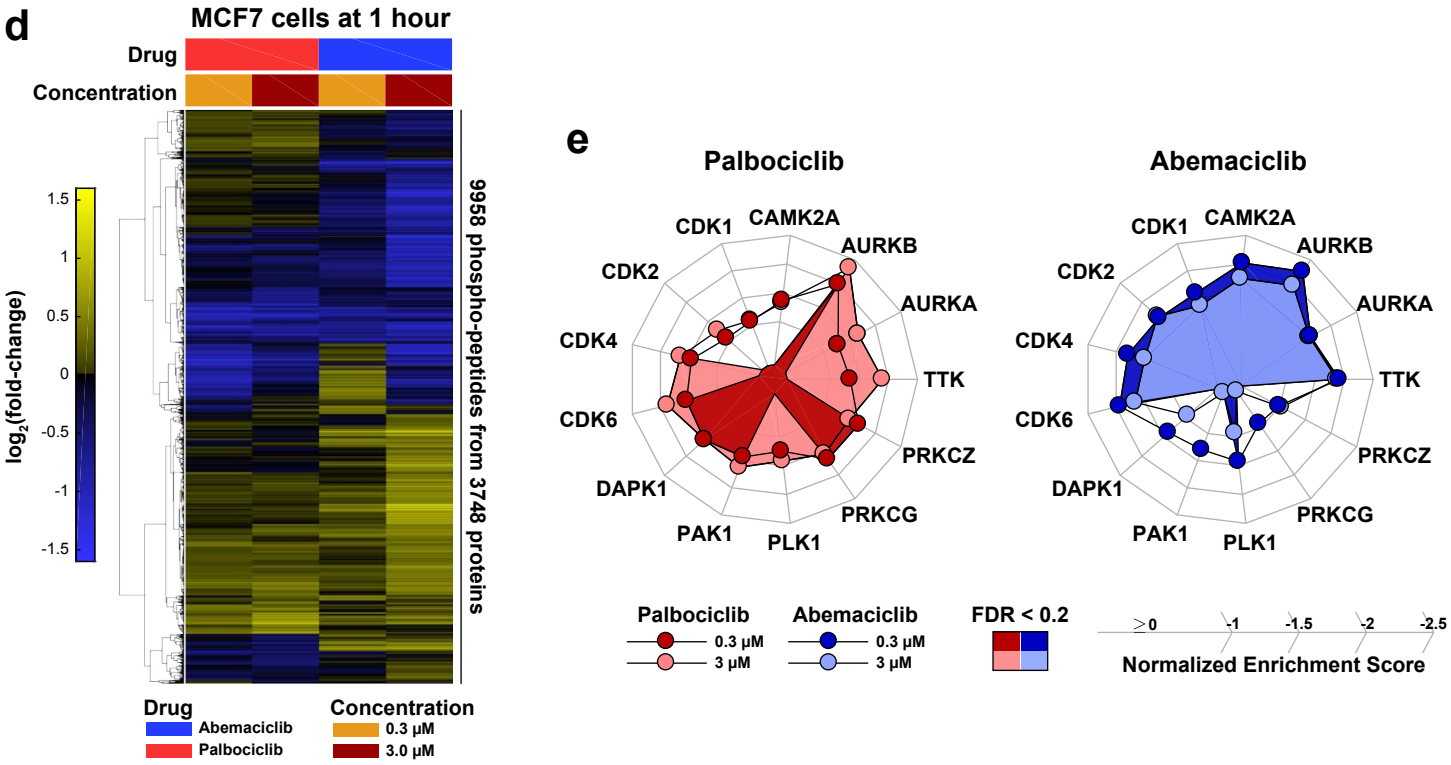

Figure 1: Molecular responses of breast cancer cell lines to CDK4/6 inhibition assayed using mRNA-Seq and phosphoproteomics. (a) Clustering of transcriptional response for seven breast cancer cell lines treated for 6 or 24 hours with ribociclib, palbociclib, or abemaciclib at the concentrations shown. Only genes for which statistically significant (FDR<0.2) changes were observed in at least 3 conditions are shown. Down-regulated genes comprised in signature 1 and 2 are outlined in red and, respectively, cyan. **(b-c)** Enrichment scores for signature 1 (b) and 2 (c) based on L1000 signatures identified by Enrichr (see Methods). **(d)** Clustering of changes in phosphopeptide levels for MCF7 cells treated for 1 hour with either abemaciclib or palbociclib at the doses indicated. **(e)** Normalized enrichment scores for kinases based on the phosphoproteomic data in panel (d). Only kinases inferred as down-regulated in at least two conditions are displayed; drugs and concentrations at which differences are significant (FDR<0.2) are shaded.

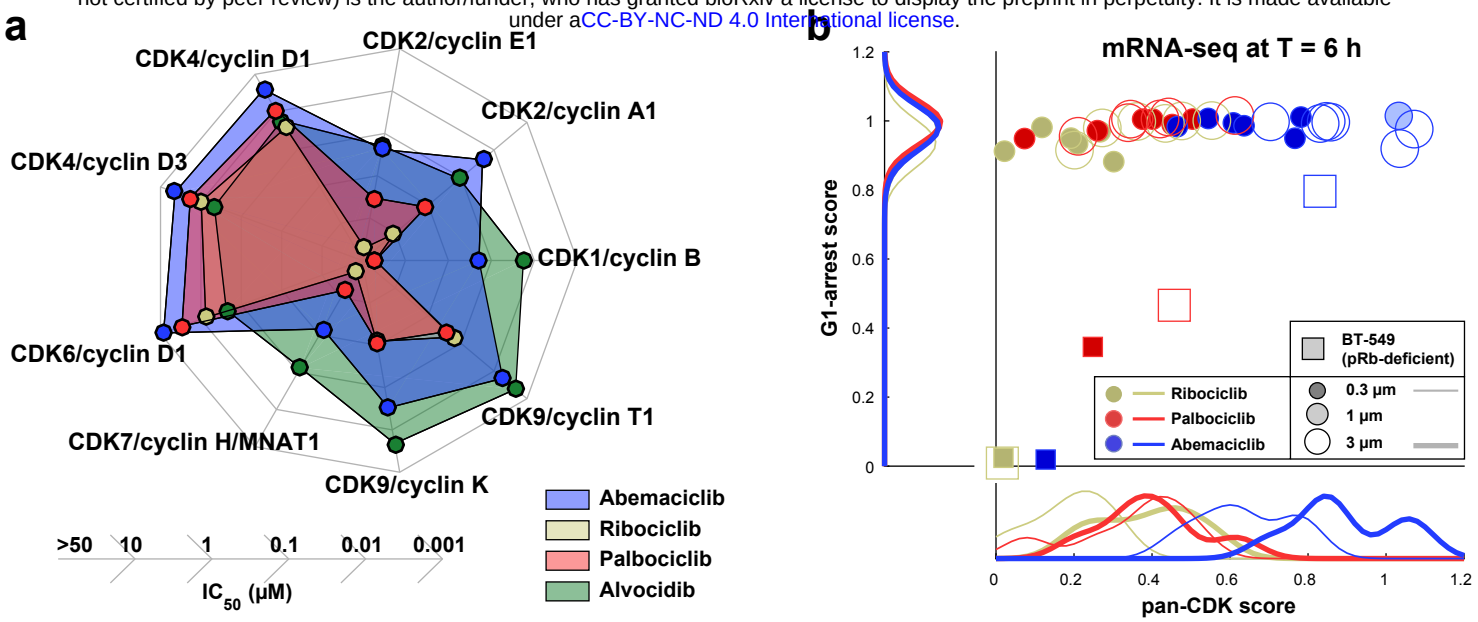

Figure 2: Extent of inhibition of CDK/cyclin complexes by abemaciclib, palbociclib, or ribociclib. (a) *In vitro* kinase activity assays confirm inhibition of additional targets by abemaciclib. Comparison of IC50 values for CDK4/6 inhibitors and alvocidib as measured using purified kinases and 10-point *in vitro* dose-response assays (see Supplementary Fig. S2). **(b)** Score of the pan-CDK transcriptional signature compared to the G1-arrest signature across all cell lines following six hours of exposure to drug. Squares represent data from pRb-deficient BT-549 cells, which are not included in the marginal distributions.

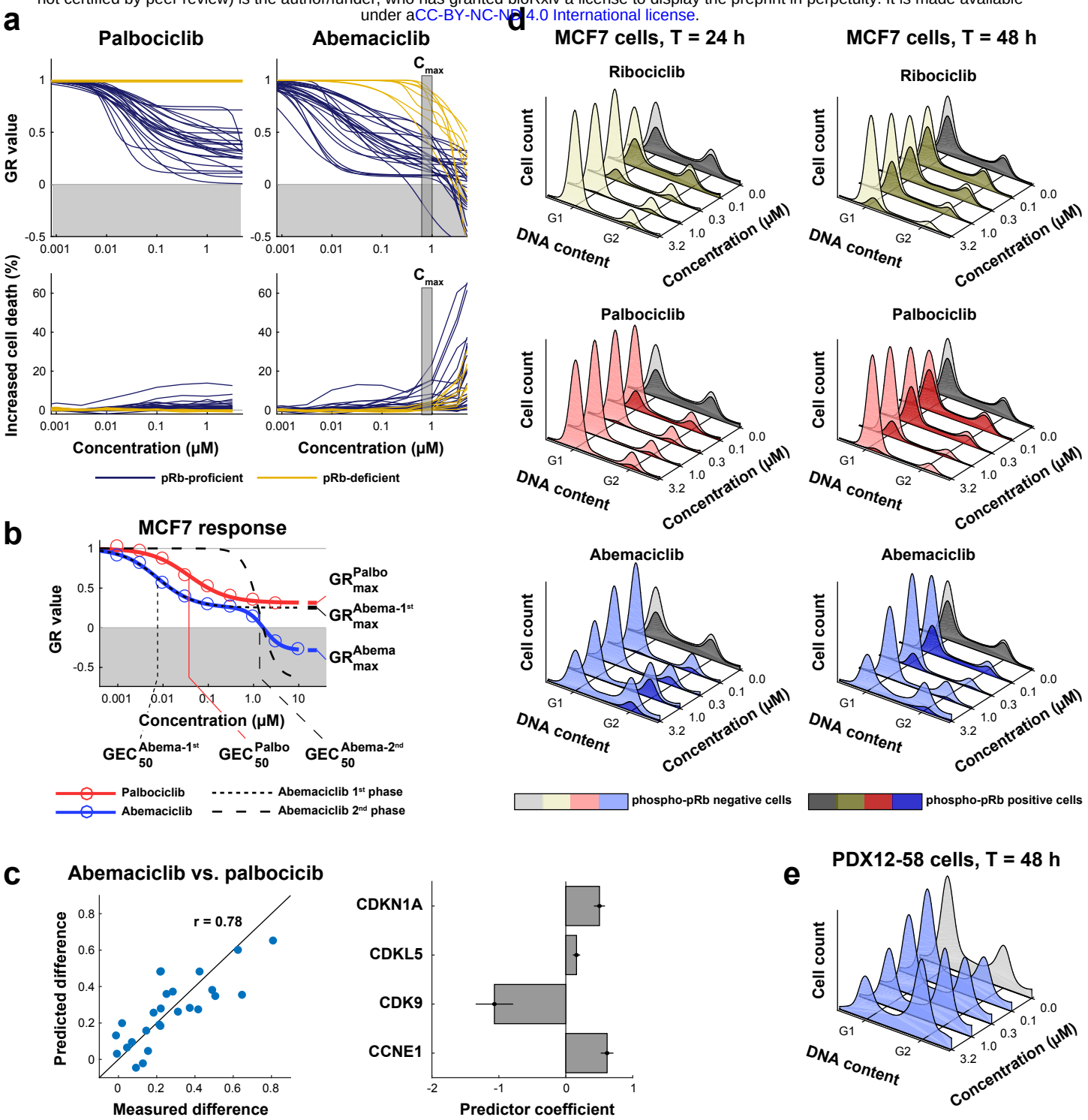

Figure 3: Comparison of the phenotypic response of breast cancer cell lines to CDK4/6 inhibitors. (a) GR curves for cell growth (top) and increased percent of dead cells over vehicle-only control conditions (bottom) for 26 pRb-proficient breast cancer cell lines (blue) and 8 pRb-deficient cell lines (yellow) treated with palbociclib (left) or abemaciclib (right) for 72 h. The vertical box illustrates the maximum serum concentration for abemaciclib (C_{max}). **(b)** Dose-response curve for palbociclib (red) and abemaciclib (blue) in MCF7 cells. Dotted lines depict two fitted sigmoidal curves whose product recapitulates the blue curve with extracted values for GEC_{50} (50%-maximal effective concentration) shown below and for GR_{max} (maximal efficacy) shown to the right. **(c)** Observed versus predicted (leave-one-out cross validation) difference in GR value at 3 μM between palbociclib and abemaciclib based on a linear model (coefficients on the right with error bars representing the standard error of the model). **(d)** Distribution of DNA content in MCF7 cells exposed to one of three CDK4/6 inhibitors at a range of concentrations for 24 (left) or 48 (right) hours. In each curve the phospho-pRb positive cell population is depicted in a darker shade. One representative replicate out of three is shown. **(e)** Distribution of DNA content for PDX12-58 cells, which are pRb-deficient, exposed to abemaciclib for 48 hours at a range of concentrations. These data represent one of three biological replicates.

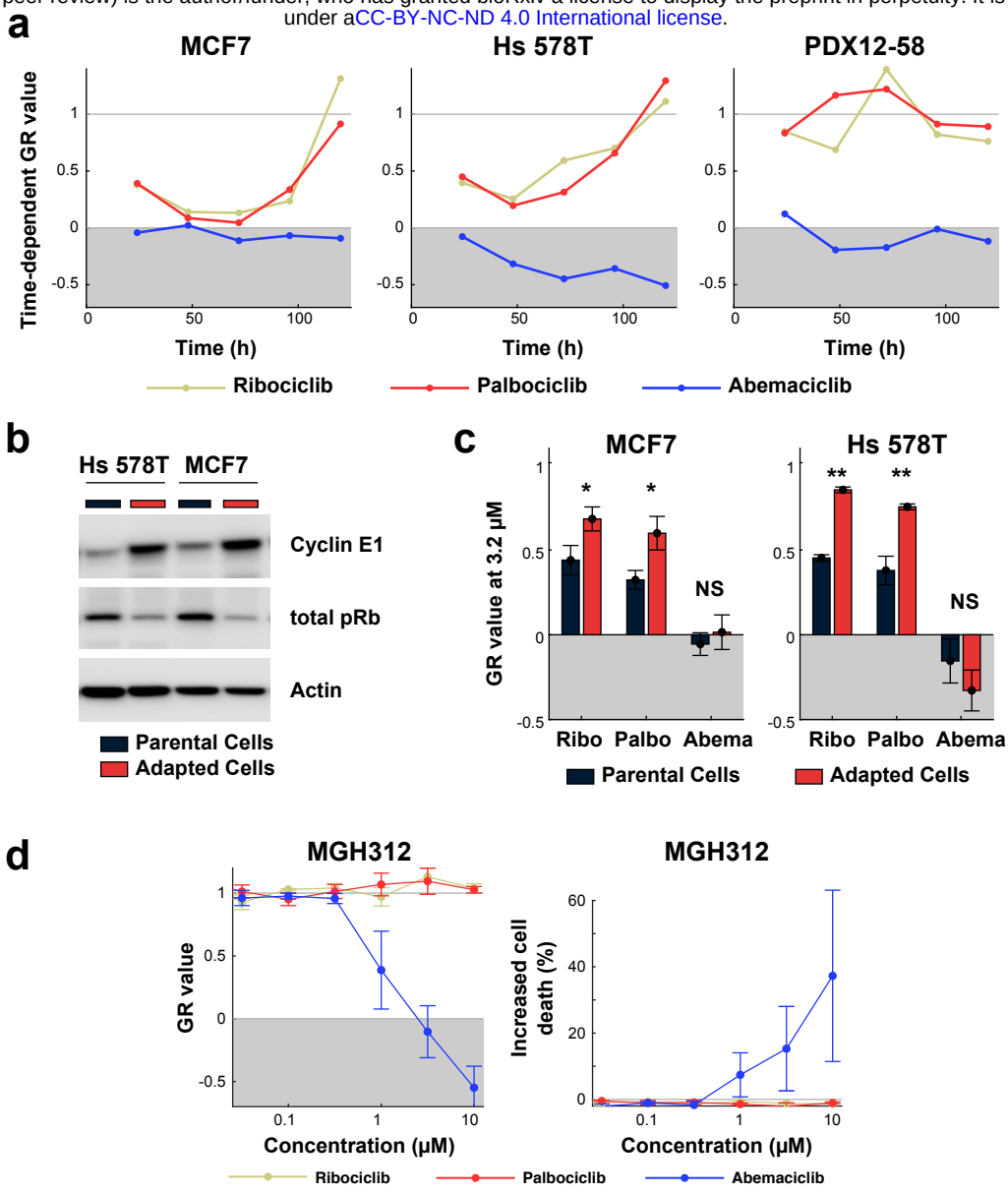

Figure 4: Acute and adaptive phenotypic responses of breast cancer cell lines and tumors to CDK4/6 inhibitors. **(a)** Time-dependent GR values for MCF7, Hs 578T, and PDX12-58 cells treated with 3.16 μM ribociclib, palbociclib, or abemaciclib for five days. One representative replicate out of four is shown. **(b)** Western Blots of cyclin E1 and total pRb levels in Hs 578T and MCF7 parental cells and cells adapted to grow in 1 μM palbociclib. **(c)** GR values for Hs 578T and MCF7 parental cells and cells adapted to grow in 1 μM palbociclib in response to treatment with 3.16 μM ribociclib, palbociclib, or abemaciclib for 72 h. * denotes $p<0.05$; ** denotes $p<0.01$ as measured using a t-test with six replicates in each group. Error bars denote SEM of six replicates. **(d)** GR values (left) and increased percent of dead cells over vehicle-only control conditions (right) for patient-derived cells MGH312 in response to 96-hour treatments with ribociclib, palbociclib, or abemaciclib. Error bars show the SEM of three replicates.

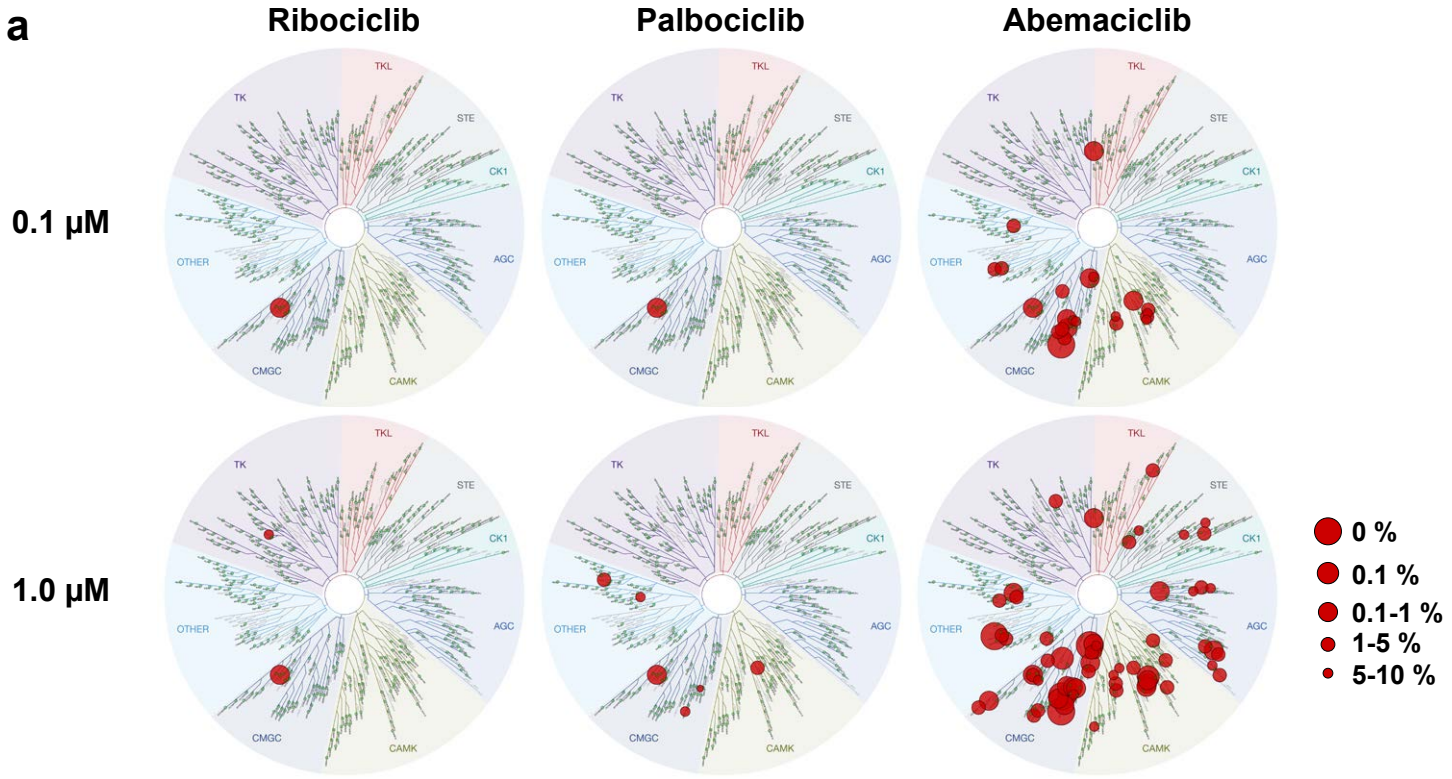

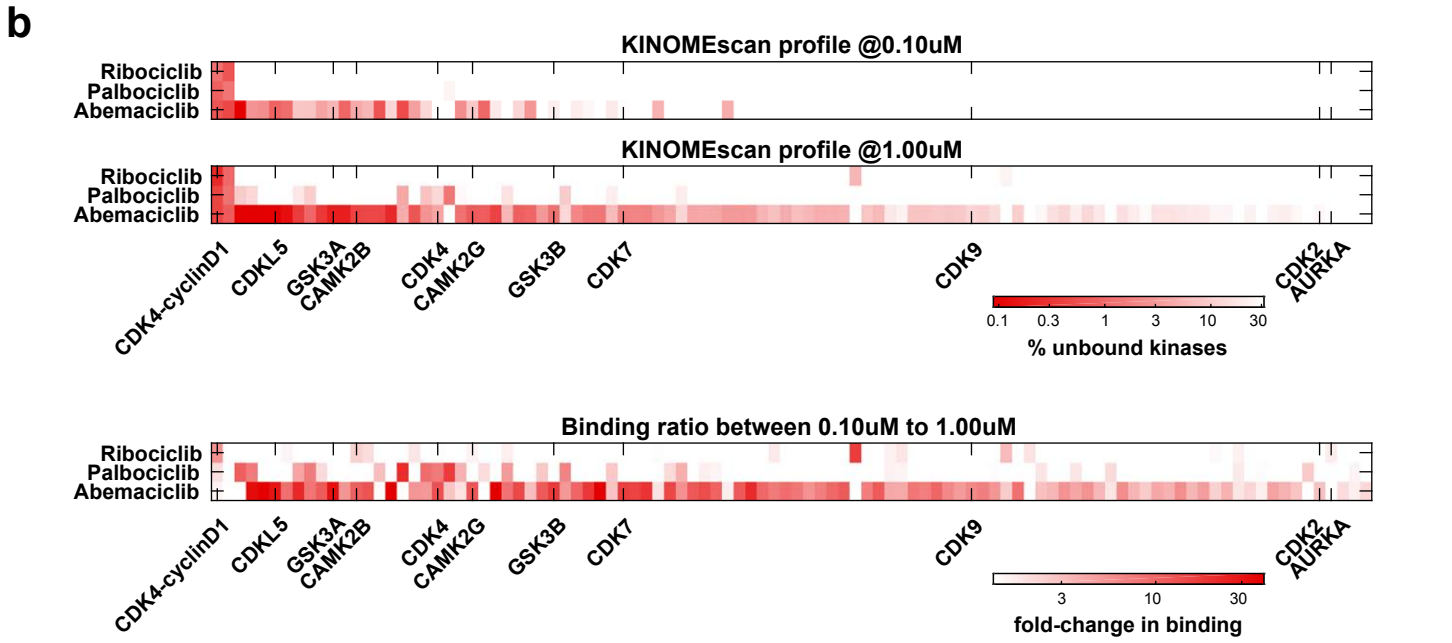

Supplementary Figure S1: KINOMEscan results for the three CDK4/6 inhibitors. (a) Kinases with less than 10% activity remaining for drug concentrations of 0.1 µM and 1.0 µM of each of the three CDK4/6 inhibitors (See Supplementary Table 11). Images generated using the TREEspot™ Software Tool and reprinted with permission from KINOMEscan®, a division of DiscoveRx Corporation, © DISCOVERX CORPORATION 2010. **(b)** Representation of the 100 most bound kinases, plus CDK2 and AURKA, for all drugs at 1 µM. The differential binding between concentrations is displayed in the bottom panel for the same kinases.

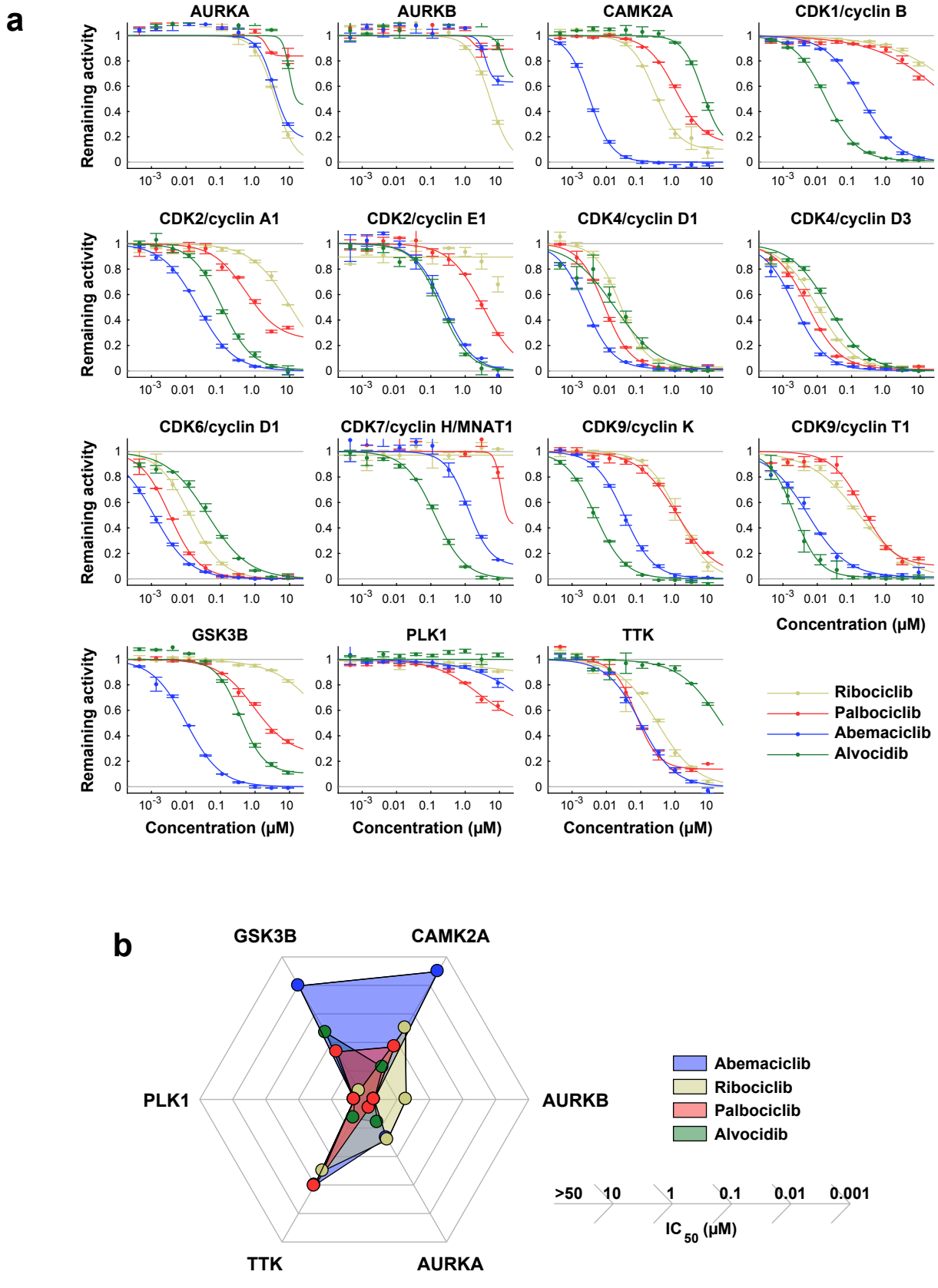

Supplementary Figure S2: In vitro activity of CDK4/6 inhibitors and alvocidib. (a) Unbound fraction or inhibition curves for select kinase targets with increasing concentrations of CDK4/6 inhibitors or alvocidib (see Methods for assay details). Error bars are the SEM of two replicates. **(b)** Comparison of IC_{50} values for CDK4/6 inhibitors and alvocidib for select kinases and CDK/cyclin complexes (see also Fig. 2a).

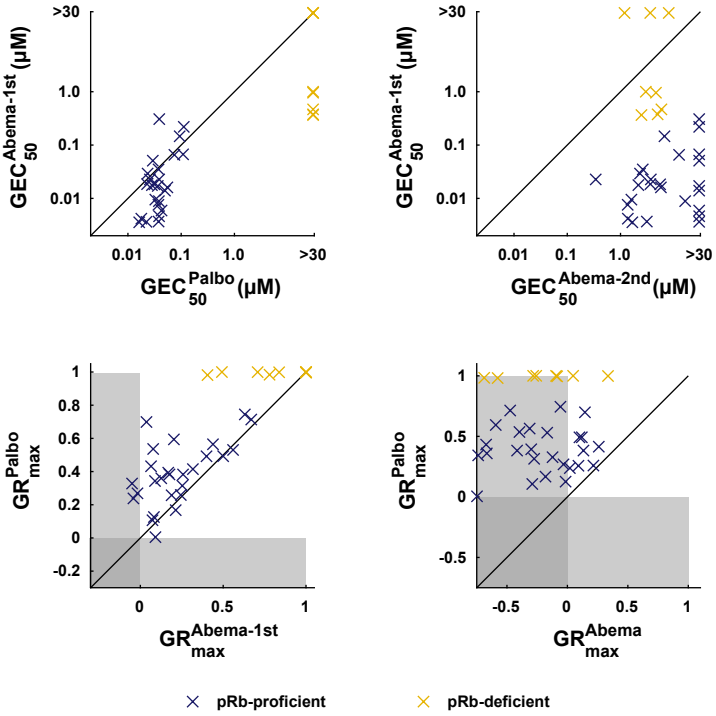

Supplementary Figure S3: Comparison of fit parameters defined in Fig. 3b for the dose response curves for palbociclib and abemaciclib shown in Fig. 3a. (top) Mid-point concentrations for palbociclib (left) and the 2nd phase of abemaciclib (right) versus the mid-point concentrations for the 1st phase of abemaciclib. (bottom) Maximal efficacy for 1st phase of abemaciclib (left) and abemaciclib (right) versus the maximal efficacy of palbociclib.

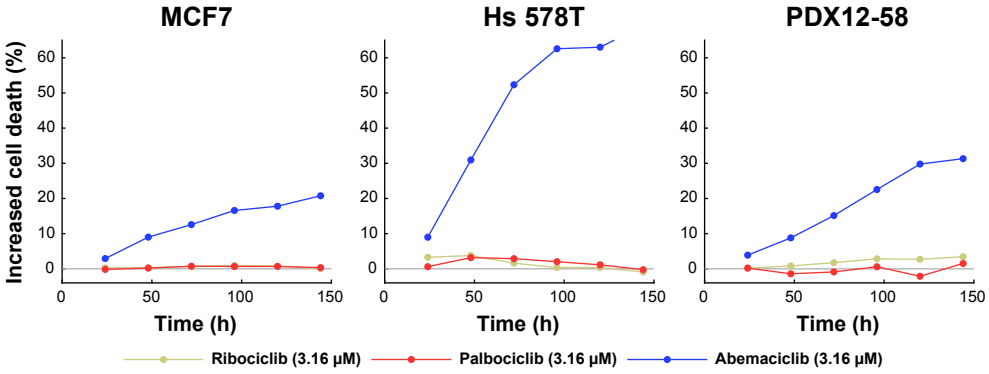

Supplementary Figure S5: Increased percent of dead cells treated with 3.16 µM ribociclib, palbociclib, or abemaciclib relative to control conditions over time (see Fig. 4a).

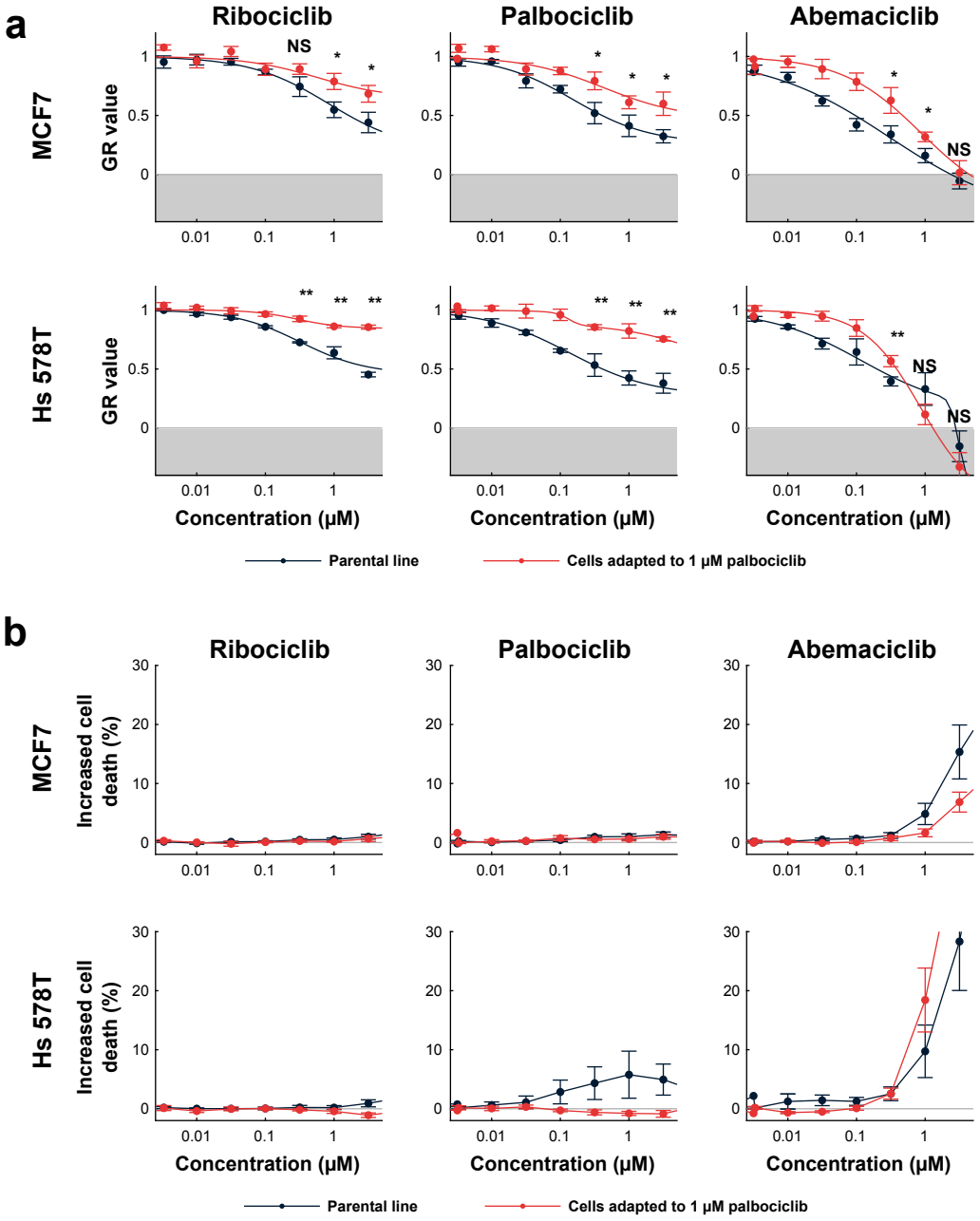

Supplementary Figure S6: Dose responses for cells adapted to grow in 1 μM palbociclib treated with increasing concentrations of CDK4/6 inhibitors. (a) GR values for cell lines adapted to grow in 1 μM palbociclib and their parental lines in response to 72-hour treatments with ribociclib, palbociclib, or abemaciclib. Error bars show the SEM of six replicates. **(b)** Increased percent of dead cells over vehicle-only control conditions for cell lines adapted to grow in 1 μM palbociclib and their parental lines in response to 72-hour treatments with ribociclib, palbociclib, or abemaciclib. Error bars show the SEM of six replicates.

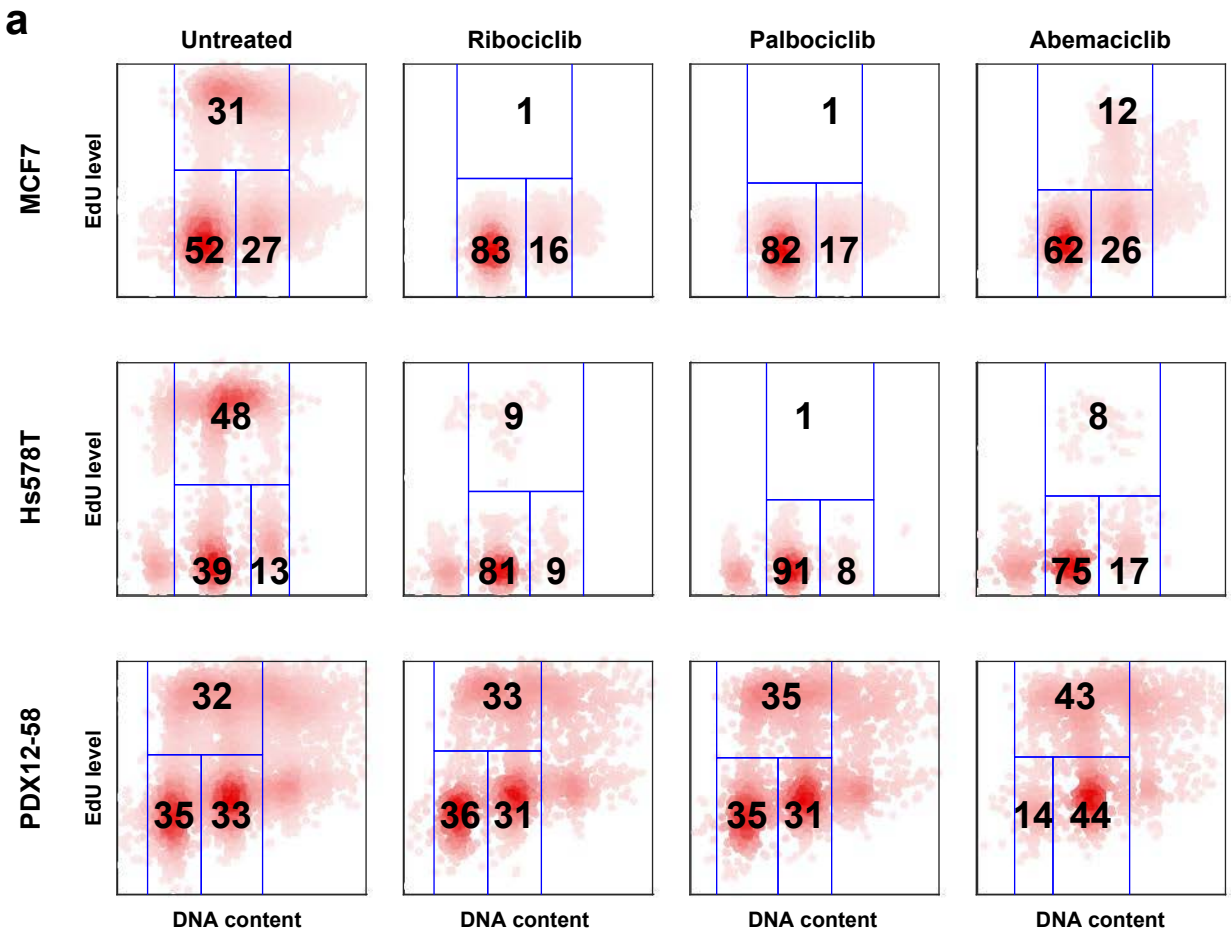

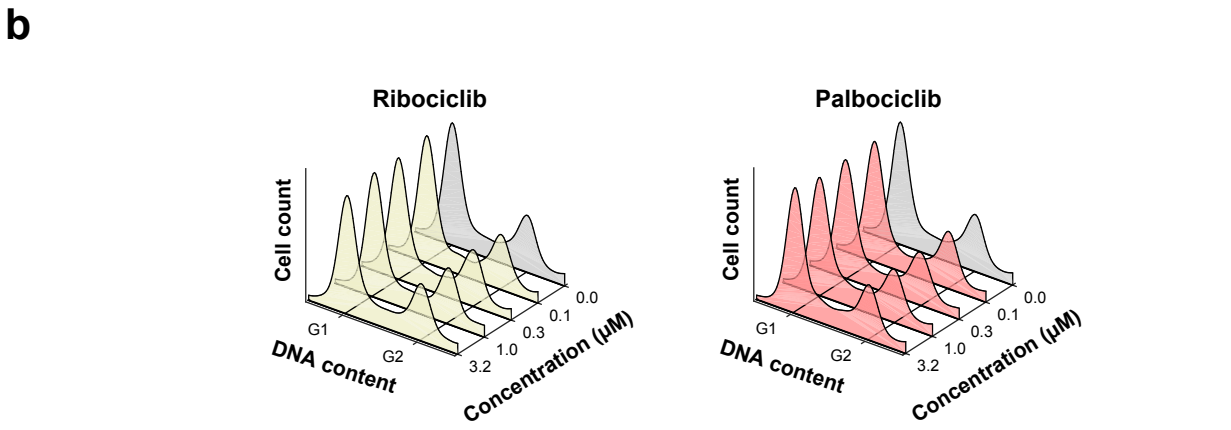

Supplementary Figure S4: Effect of CDK4/6 inhibitors on the distribution of cells through the cell cycle. (a) DNA content versus EdU intensity for three breast cancer cell lines either untreated or treated for 24 hours with 1.0 μM of ribociclib, palbociclib, or abemaciclib (from left to right). Color intensity reflects density of cells; numbers represent the percentage of cells in each phase of the cell cycle based on automated gating (blue lines). **(b)** Distribution of DNA content for PDX12-58 cells, which are pRb-deficient, exposed to either ribociclib or palbociclib for 48 hours at a range of concentrations. These data represent one of three biological replicates.

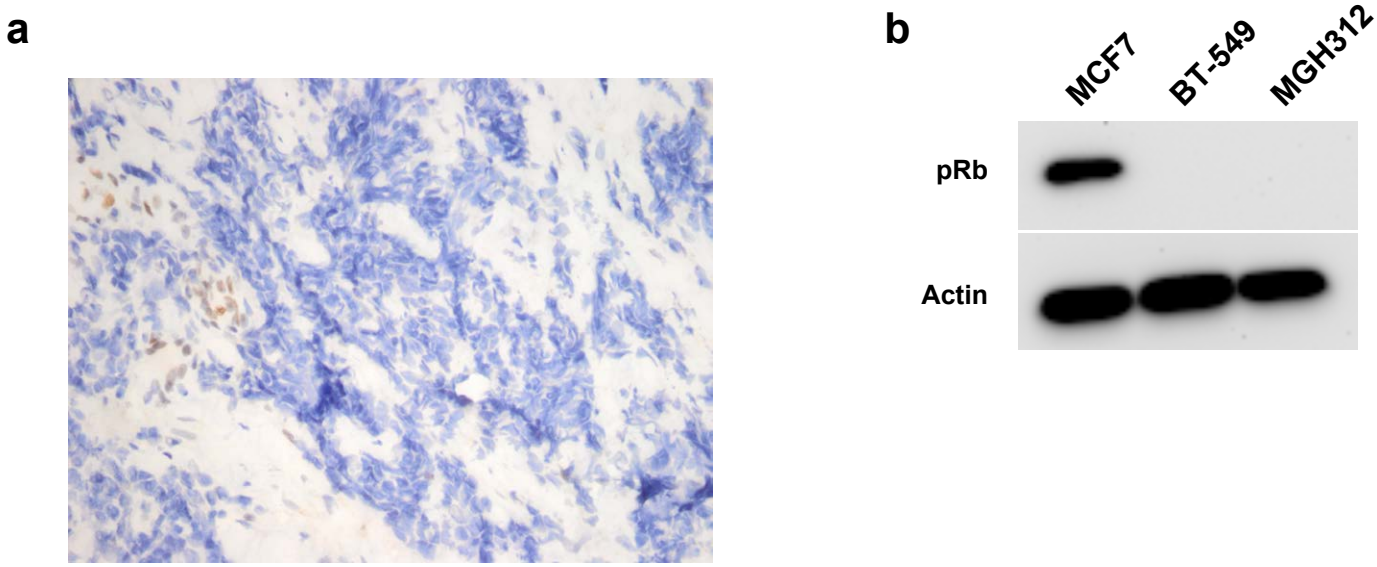

Supplementary Figure S7: pRb status of patient sample and derived line. (a) pRb immunohistochemistry staining of patient biopsy at the site from which the cell line MGH312 was derived. **(b)** Western Blot of pRb for MCF7, BT-549, and MGH312 cells.